Tailoring frequency combs through VCSEL polarization dynamics

Yaya Doumbia, Delphine Wolfersberger, Krassimir Panajotov, Marc Sciamanna

Tailoring frequency combs through VCSEL polarization dynamics

YAYA DOUMBIA,[1,2*] DELPHINE WOLFERSBERGER, [1,2] KRASSIMIR PANAJOTOV,[3,4] AND MARC SCIAMANNA [1,2]

[1] *Chaire Photonique, CentraleSupélec, LMOPS, 2 Rue Edouard Belin 57070 Metz, France*
[2] *Université de Lorraine, CentraleSupélec, LMOPS, 2 Rue Edouard Belin 57070 Metz, France*
[3] *Brussels Photonics Group (B-PHOT), Vrije Universiteit Brussel, Brussels, Belgium*
[4] *Institute of Solid State Physics, Bulgarian Academy of Sciences, Sofia, Bulgaria*
[*] *yaya.doumbia@centralesupelec.fr*

Abstract: We investigate experimentally the nonlinear polarization dynamics of a VCSEL subject to optical injection of a frequency comb. By tuning the polarization of the injected comb to be orthogonal to that of the VCSEL, we demonstrate the generation of either a single polarization or a dual polarization frequency comb. The injection parameters (Injected power and the detuning frequency) are then used either to generate harmonics of the initial comb spacing, or to increase the number of total output frequency lines up to 15 times the number of injected comb lines. Optimisation of the injection parameters yields a comb extending over 60 GHz for a comb spacing of 2 GHz with a Carrier to Noise Ratio (CNR) up to 60 dB. Our technique allows to separately control the comb spacing and comb bandwidth, CNR and polarization. Our finding can be used for spectroscopy measurement and also for polarization division multiplexing in optical data communications.

1. Introduction

Since the demonstration of applications in optical metrology, optical telecommunication and gas spectroscopy, optical frequency comb (OFC) technologies have driven significant attention. The required OFC properties such as comb bandwidth, comb spacing, and Carrier to Noise Ratio (CNR) change from an application to another one. To satisfy each application requirements, several methods of OFC generation have been reported recently including, quantum cascade laser [1], mode locking laser [2] micro-resonators [3] and electro-optics modulators [4]. Each of these techniques presents many advantages but with some limitations that has to be improved. For example, mode locking laser and quantum cascade laser can generate stable and ultra-broadband combs, but the comb spacing depends on the cavity properties. Micro-ring resonators can generate a stable broadband OFC, but with significant fluctuation in amplitude. An OFC based on electro-optics modulators has the advantage of tunable comb spacing, but the modulator induces significant insertion loss. Yet to date, generating an OFC that exhibits large bandwidth with tunable comb spacing and high carrier to noise ratio (CNR) is still challenging. Here, we propose a new approach of broad OFC generation that offers the possibility to adapt the comb properties to applications ranging from optical telecommunication to gas spectroscopy, exploiting the VCSEL polarization dynamics.

Vertical cavity surface-emitting laser (VCSEL) has attracted much attention in the last decades due to their numerous applications such as optical communication and sensing [5–8]. Beyond these applications, VCSELs offer the advantage of compactness, low cost, and low energy consumption and opens the possibility of mass production. The cylindrical geometry of the VCSEL cavity, together with symmetry of the gain in the quantum wells plane, leads to a weak polarization anisotropy with the selection of two preferential orthogonal polarization directions. The VCSEL output is typically linearly polarized on one of the two orthogonal directions. Under

certain conditions, polarization switching (PS) between the orthogonal polarization modes may occur. Several techniques have been used to observe PS in VCSEL, including controlling the operating temperature and the injection current. Beyond the PS, VCSELs can exhibit rich nonlinear polarization dynamics under optical injection or current modulation [9–14]. It has been demonstrated recently that VCSEL, even in free-running, may show complex polarization dynamics [15].

One specific technique to explore the nonlinear dynamics and the polarization properties of the VCSEL is the optical injection. The light from an external laser called master laser is injected into the cavity of the VCSEL, which promotes the appearance of more complex dynamics. The optical injection has been used to highlight several varieties of nonlinear dynamics in VCSEL such as wave-mixing, frequency pulling, time-periodic, and chaotic polarization dynamics [5]. Beside the injection parameters (injected power and detuning frequency), the polarization of the injected light is then an additional technique to induce and control PS and its corresponding bistability [5, 10, 11, 16–19]. The PS bistability refers to the situation where for fixed detuning, the PS occurs at two different levels of injected power [5]. It can also be observed for fixed injected power when varying the detuning frequency. The present work addresses the polarization dynamics of VCSEL when it is submitted to a modulated optical injection such as the one from an OFC. Indeed, satisfying the demand for the growth of bandwidth in optical communication has become a challenge in the last decade. Coherent Wavelength Division Multiplexing is a technique in which an OFC is used to transmit data (CoWDM) [20]. One of the main challenges of CoWDM technologies is demultiplexing OFC with narrow comb spacing. To this end, the optical injection of the comb into a single-mode laser has been used to select and amplify a comb line [21]. The dynamics induced by a modulated signal in a single-mode diode laser has been attracting much attention recently [22–24, 24, 25]. Recent works have shown that instead of selective amplification, the laser bifurcates to the generation of sub harmonics [26] or a new wideband comb solution that has some properties in common with the injected comb [27–29]. Harmonic OFC generation with diode laser subject to comb injection may be a useful tool for spectroscopy measurement [30]. Gain switching of a semiconductor laser is another technique to generate an OFC that may improve with optical injection [31]. Recent experimental and theoretical analysis of polarization dynamics of VCSEL demonstrated the possibility of generation of two polarization comb which can enlarge the overall comb under gain switching [32, 33]. The polarization combs properties have been found to improve with orthogonal, parallel, or arbitrary optical injection into the comb. Unfortunately, the performance of these polarization combs obtained by gain switching depends strongly on the modulation frequency [34]. The question of how a polarized OFC injection into a single-mode VCSEL can impact its polarization dynamics is therefore of fundamental and applied interest and has not been addressed so far.

More specifically, we study the nonlinear dynamics of a single longitudinal mode VCSEL subject to optical injection from an OFC. Injection locking is due to the coupling between oscillators provided by the transmission from an external oscillator (the master) to an internal oscillator (the slave). Optical injection locking only occur if the difference between the frequencies of the master and slave lasers is sufficient small, i.e., they are within a certain bandwidth known as the locking region. The optical injection locking with the frequency comb is characterized by the selective amplification of the comb line that shows the smallest detuning frequency from the injected laser. Optical phase locking relates to a laser that emits at a frequency which is fixed with respect to that of another laser. The optical phase locking can be realized using several techniques such as optical phase lock loops and optical injection locking. Throughout this work, the optical injection locking refers to the frequency locking between the injected comb and the injected laser. The optical injection with an OFC has attracted more attention due to its ability to select and amplify a desired comb line through the injection locking technique [35, 36]. Beyond the injection locking with selective amplification reported in [37–39], we hereby reveal several

bifurcations scenarios leading to stable unlocked time-periodic dynamic corresponding to a new OFC with the same comb spacing as the injection one, but with a significantly extended bandwidth, an improved Carrier to Noise Ratio (CNR), and a controllable polarization. The optical injection parameters(Injected power and the detuning) are varied to control the comb spacing through the generation of the harmonics OFC. Some specific detuning frequencies are found to lead to dual orthogonal polarized unlocked time-periodic dynamics corresponding to dual-frequency comb. These orthogonal polarization combs correspond to two distinct multiple transmission channels which could simplify the standard polarization division multiplexing scheme by suppressing of optical devices used to separate the channels. The impact of the OFC parameters on the polarization of the injected VCSEL is analyzed in detail. The quality of the resulting comb is therefore tailored by the injection parameters. Very recently, harmonics comb lines generation has been used to discretely control the soliton frequency comb spacing between 3.23 GHz and 19.38 GHz [40]. Also OFC from diode laser have recently been reported with comb spacing ranging from several GHz to THz [41]. These combs are useful for optical communication networks, but can not be applied for spectroscopy applications which require comb spacing smaller than 1 GHz. Our results demonstrate very stable OFCs whose comb spacing can be adjusted to adapt to optical communication networks or spectroscopy applications. Interestingly, our technique allows to control the comb spacing either through harmonics comb generation or by the injected modulated field. The bandwidth of the resulting comb is increased through nonlinear dynamics to achieve 15 times that of the injection comb. In addition, the CNR which characterizes the power in the comb lines has increased to reach 60 dB, which is more than 3 times the one obtained very recently [42] and larger than the one required for spectroscopy [43].

2. Experimental setup

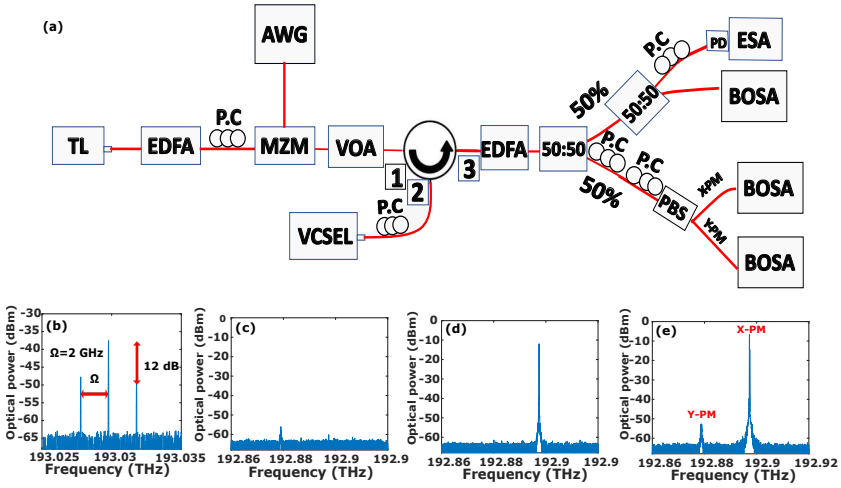

Fig. 1. Set up for OFC injection into a VCSEL. TL: Tunable Laser, EDFA: amplifier, PC: Polarization Controller, AWG: Arbitrary Waveform Generator, MZM: Mach-Zehnder Modulator, VOA: Variable Optical Attenuator, BOSA: Brillouin Optical Spectrum Analyser, PD: photodiode, ESA:electrical spectrum analyser ,Figure 1 (b) Optical spectra of the injected comb with a comb spacing of $\Omega = 2$ GHz. Figure 1 (c), (d) and (e) correspond to the polarization resolved optical power of Y-PM, X-PM and the total output, respectively.

In Fig. 1 (a) we show the experimental setup for the optical injection. A continuous-wave (CW) tunable laser (Yenista Tunics T100S) is amplified by an Erbium-Doped Fiber Amplifier

(EDFA) and sent to a $LiNbO_3$ Mach-Zehnder (MZ) Modulator with a 12.5 GHz bandwidth. The linewidth of the tunable laser is around 30 MHz. The temperature is kept fixed at 23°C. The minimum step of frequency we can achieve on the tunable laser is 0.01 GHz. The polarization controller (PC) at the input of the MZ Modulator allows to align its input with the polarization of the tunable laser. An electric signal modulation is generated by an Arbitrary Waveform Generator (AWG) (Tektronix AWG 700002A) and sent to the RF port of the MZ Modulator. At the output of the MZ Modulator, an OFC with lines of different level of power is generated. The total optical power of the comb lines is controlled with a Variable Optical Attenuator (VOA). The injected laser is a single-mode VCSEL which is biased at a current of I=6 mA corresponding to 2 times the threshold current. At this current, the total output power and the relaxation oscillation frequency (ROF) have been measured to be P_{VCSEL} = 330 μW and ROF = 4.2 GHz, respectively. The dominant Polarization Mode (X-PM) emits at ∼ 1553.8 nm. A fiber circulator is arranged to provide isolation for the VCSEL injection. The polarization controller at the input of the VCSEL allows to control the polarization of the injected light. To make sure that the polarization of the injection matches with the Y-polarization of the VCSEL, we analyze the dynamics of the VCSEL. When the polarization of the injection matches with that of the VCSEL, the injected power required to achieve the injection locking is the smallest. We set the detuning to zero from Y-PM and adjust the polarization such that injection locking is achieved for minimum injected power. An amplifier (EDFA) is used to amplify the VCSEL output. An optical coupler is used to split the light in two paths with equal power. The first path is used to analyze the nonlinear dynamics of the total output power of the VCSEL with a high-resolution optical spectrum analyzer BOSA 400, which allows monitoring optical spectra with a resolution of about minimum 0.1 pm at the operating wavelength of 1550 nm. We examined the power spectrum on an electrical spectrum analyser (ESA). The power spectrum was analyzed using an electrical spectrum analyser (ESA). In the second path, two consecutive polarization controllers are used to provide maximum alignment between the linear polarization modes of the VCSEL and the axes of the polarized beam splitter (PBS) to discriminate the linear polarization modes and observe them in separate optical spectra on the BOSA. In this study, we will consider Ω to be the comb spacing in GHz

Figure 1 (b) shows the optical spectrum of the injected comb for a fixed comb spacing (Ω = 2 GHz). The difference between the power of the central comb line and the side comb lines is around 12 dB. Figure 1 (c) shows the optical spectrum of the depressed polarization optical power (Y-PM) of the VCSEL in the free running regime. The maximum power of this polarization mode is around -53 dBm. Figure 1 (d) shows the optical spectrum of the dominant polarization (X-PM) of the VCSEL in the free-running regime. This polarization mode emits with a maximum power of around -10 dBm. Figure 1 (e) presents the optical spectrum of the total output power of the VCSEL in free running. The difference between the frequency of the linear polarization modes which correspond to the VCSEL birefringence is around 17.71 GHz at 23 ° C. In the following, the frequency detuning $\Delta\nu$ is defined from the frequency of the central comb line to the frequency of VCSEL X-PM i.e., $\Delta\nu = \nu_0 - \nu_x$, where ν_0 and ν_x are the frequencies of the central injected comb line and the X-polarization mode of VCSEL (X-PM), respectively. The x-axes of the optical spectra will show the relative frequency with respect to the X-polarization mode (X-PM),i.e., the zero value on x-axis will match with the frequency position of X-polarization mode (X-PM).

3. Polarization switching curves

In Fig. 2, we analyze the evolution of the polarization switching power when the injected power is increased and decreased for a fixed detuning frequency of $\Delta\nu = \nu_0 - \nu_x$. We consider polarization switching when the difference between the power in Y-PM and X-PM modes is more than 30 dB. The main goal is to evaluate the impact of the comb injection on the polarization switching bistability. To this end, we compare in the plane of injection parameters the polarization switching

on-power and off-power for both a single-mode injection and a OFC injection. The mappings in Fig. 2 correspond to the comparisons of the PS curves for injection of: (a) a single-mode and a comb with comb spacing of 500MHz, (b) two combs of 500MHz and 2 GHz comb spacing, and (c) two combs of 2 GHz and 4 GHz comb spacing. The frequency detuning is $\Delta\nu = 0$ GHz and $\Delta\nu = -17.7$ GHz, respectively, corresponding to the situations in which the central injected comb line matches the X-PM and the Y-PM frequency positions. By zero detuning, we mean a detuning at the minimum value that can be achieved considering the minimum frequency step of the tunable laser. These figures show that OFC injection influences both switching and polarization bistability.

The width of the bistability region for detuning smaller than -17.7 GHz, i.e., negative detuning from Y-PM, is larger than the one for positive detuning in the single-mode and comb injection cases, which is in good agreement with the observations made for single mode injection [16]. For negative detuning from Y-PM, i.e. $\Delta\nu < 17.7$ GHz, the injected power required to achieve polarization switching is smaller for a comb injection than for a single-mode injection and decreases with the increase of the injected comb spacing. When the detuning is larger than -17.7 GHz, i.e., positive detuning from the Y-PM, the power required to switch is larger for a comb injection than a single-mode injection. Figures 2 (b) (Ω = 500 MHz and Ω = 2 GHz comb spacing) and (c) (Ω = 2 GHz and Ω = 4 GHz comb spacing) show that there is no simple linear dependence between the increase of the comb spacing and the increase of the switching power. PS leads to different dynamics that depend on the injection parameters. The red arrows in the mapping of Fig. 2 (b) indicate different bifurcations scenarios for which an in-depth analysis will be made in the following.

An example of a OFC obtained from optical injection is given in Fig. 3, where we present the polarization-resolved spectra for a fixed comb spacing of Ω = 2 GHz. At this injected power (P_{inj} = 183.3 μW) and detuning ($\Delta\nu = -10.53$ GHz), the VCSEL has switched from the dominant polarization mode to the normally depressed polarization mode. The polarization modes are split by using two polarization controllers and a polarized beam splitter (PBS). Figure 3 (a), (b) and (c) show the optical spectra of X-PM, Y-PM and the total output power. OFCs are observed in the optical spectra of the Y-PM [Fig. 3 (b)] and the total power [Fig. 3 (c)]. The red arrow in the box in Fig. 3 (a) indicates the residue of the X-PM due to the spontaneous emission. Interestingly, not only the polarization of the resulting comb has changed from that of the injected comb, but also the properties of the comb have been modified when compared to the injected comb.

4. Polarized frequency comb generation

The comb shown in Fig. 3 emerges from a series of bifurcations which we now analyze.

We first analyze the nonlinear polarization dynamics of the VCSEL in the plane of injection parameters indicated by the red arrow with letter A in Fig. 2 (b). Figures 4 (a)-(h) show the sequence of bifurcations to polarization switching with generation of an extended and polarized comb. These figures are obtained for a fixed comb spacing of Ω = 2 GHz and detuning of $\Delta\nu = -10.78$ GHz. For a low injected power, P_{inj} = 0.3 μW, the VCSEL is still emitting in the X-PM mode without any excitation of the Y-PM mode (Fig. 4 (a)). The red arrow in the optical spectrum indicates the position of the central injected comb line. An increasing of power leads to an excitation of the two polarization modes as shown in Fig. 4 (b). The polarization mode that shows the maximum gain is still the X-PM but the level of power in Y-PM is increasing when the injected power is increasing. From Fig. 4 (b), a small increase in injected power is sufficient to observe the polarization switching as shown in Fig. 4 (c). This polarization switching is accompanied by a complex dynamic with a maximum peak at the free-running frequency position of Y-PM. The X-PM is strongly suppressed with a ratio of suppression around -50 dB. When we increase again the injected power, the complex dynamic gives rise progressively to a

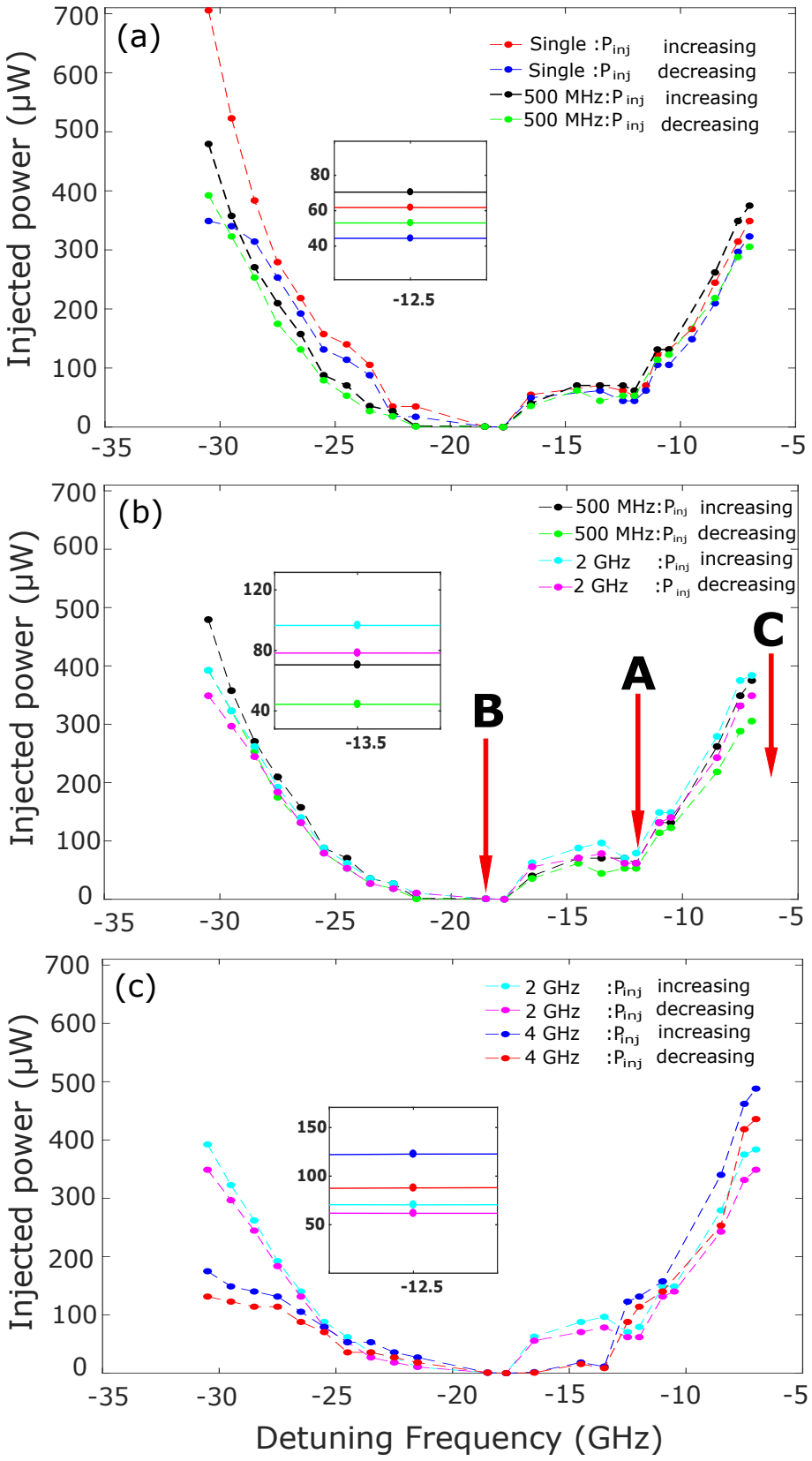

Fig. 2. Mapping of polarization switching bistability in the plane of injection parameters for single and OFC injection. In the map, we analyse the switching curves when increasing the injected comb spacing. (a) single-mode and 500 MHz comb injection , (b) 500 MHz and 2 GHz comb injection, and (c) 2 GHz and 4 GHz comb injection.

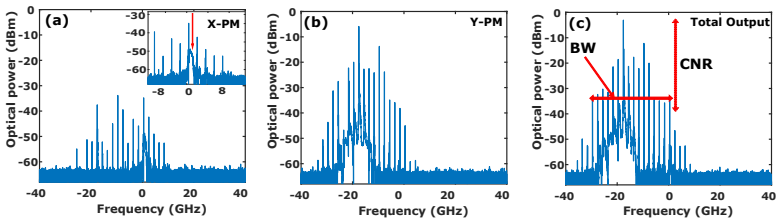

Fig. 3. Optical spectra for each polarization and total output power of the VCSEL showing the sequence of bifurcation leading to a broad OFC generation for fixed $\Omega = 2$ GHz and detuning $\Delta\nu = -10.53$ GHz. (a), (b) and (c) polarization resolved comb for X-PM, Y-PM, and the total output, respectively at $P_{inj} = 183.3$ µW. The horizontal and vertical double arrows in (c) indicate the way to calculate the bandwidth (BW) and the carrier to noise ratio (CNR), respectively. The CNR corresponds to the amplitudes of the comb lines from the noise level. The BW is measured by considering the comb lines above -30 dB from the maximum amplitude.

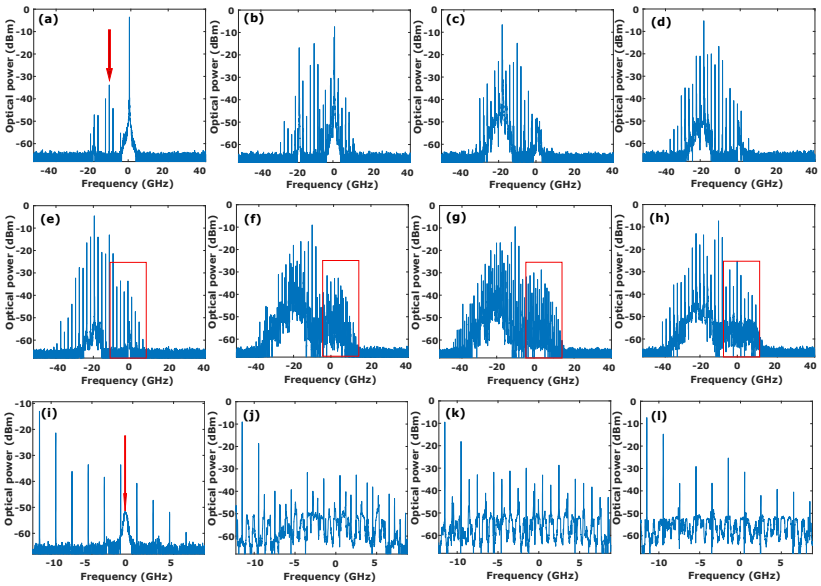

Fig. 4. Scenario A: Optical spectra for fixed comb spacing $\Omega = 2$ GHz and detuning $\Delta\nu = -10.78$ GHz when varying the injected power P_{inj}. (a), (b) unlocked dynamics at $P_{inj} = 0.3$ µW, $P_{inj} = 64$ µW, respectively, (c) PS with complex dynamics at $P_{inj} = 95.7$ µW , (d) and (e) Unlocked time-periodic dynamics corresponding to an OFC at $P_{inj} = 100.5$ µW and $P_{inj} = 113.1$ µW, respectively, (f) and (g) harmonics at third and half of comb spacing in both polarization modes at $P_{inj} = 352$ µW, and $P_{inj} = 440$ µW, and (h) Unlocked time-periodic dynamics in both polarization modes corresponding to an OFC at $P_{inj} = 688$ µW. The optical spectra in (i), (j), (k), and (l) represent zooms of the optical spectra in (e), (f), (g), and (h), respectively. The red arrows in the optical spectrum of (a) and (i) indicate the position of the central injected comb line and the residue of X-polarization mode after PS due to the noise of spontaneous emission.

broad OFC with the same repetition rate as the injected comb as shown in Fig. 4 (d). This comb has an important noise pedestal that decreases with the injected power to give the one in Fig. 4 (e). This is also accompanied by an increase in the number of comb lines. The strong lines in the optical spectra in Fig. 4 (d) and (e)) appear at the position of the free-running frequency of the Y-PM of the VCSEL. The window box in Fig. 4 (e) is magnified in Fig. 4 (i). We observe that the comb lines are well regularly spaced. The red arrow in the spectrum of Fig. 4 (i) indicates the residue of X-PM due to the spontaneous emission noise. An increase in power destabilizes the comb and complex dynamics takes place in both polarization modes. A fine-tuning of injected power leads to harmonics comb in Figs. 4 (f) and (g). The window box in Fig. 4 (f) and (g) is magnified in Fig. 4 (j) and (k), respectively. Figures 4 (j) and (k), show that the optical spectra in Fig. 4 (f) and (g), correspond to harmonic combs at third and half of the injected comb spacing, respectively. Harmonic OFC has previously been observed [22, 26], but for larger comb spacing. When increasing the injected power from Fig. 4 (f) to Fig. 4 (g), complex polarization dynamics is observed in both polarization modes. For some values of injected power, the laser output is quite close to harmonic OFC at a quarter of the injected comb spacing. When further increasing the injected power, the harmonic comb bifurcates to two polarization OFCs with the total output power corresponding to a broad OFC [Fig. 4 (h) and the corresponding zoom in (l)]. Increasing the injected power the initial comb (a) has changed to a single polarization (e) or a two polarization (h) frequency comb.

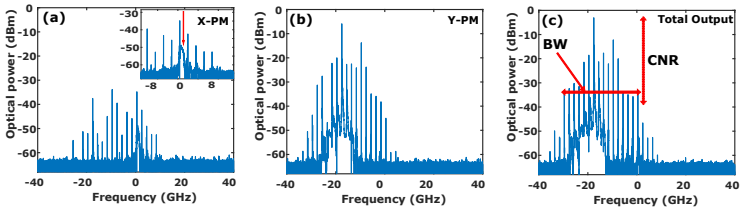

Fig. 5. Polarization resolved optical spectra corresponding two polarization comb involution in Scenario A. (a), (b), (c), optical spectra of X-PM, Y-PM and total output power, respectively for fixed $\Delta\nu = -10.78$ GHz and $P_{inj} = 680$ µW. In the frequency axis of the optical spectra, the zero value matches with the frequency position of the dominant polarization mode (X-PM)

An example of polarization-resolved of an OFC obtained from bifurcation scenarios A describe in Fig. 4 (h) is shown in Fig. 5. Figure 5 (a), (b), and (c) present the optical spectra corresponding to X-PM, Y-PM, and total output power, respectively. In the frequency axis of the optical spectra, the zero value matches with the frequency position of the dominant polarization mode (X-PM). We observe an OFC in both polarization modes, which combine to give rise to an overall OFC in the total output power. The CNR of the X-PM is around 30 dB which is controllable with the injection parameters.

Figure 6 shows additional sequence of bifurcations when doing a sweep of the detuning frequency for a fixed injected comb spacing of $\Omega = 2$ GHz and fixed injected power of $P_{inj} = 150$ µW. In Fig. 6 the top and the bottom panels correspond, respectively, to the optical spectra and to their zooms. When varying the detuning, the VCSEL output shows an unstable comb (not shown) with the presence of frequency lines like the ones in Fig. 4 (c). The instability gradually decreases to give rise to an OFC with the same repetition rate as the injected comb as shown in Fig. 6 (a_1). The new comb solution remains stable over a certain range of detuning and starts to deteriorate with the appearance of new frequency lines around the main comb lines leading to complex harmonics comb dynamics in Fig. 6 (a_2). These dynamics are close to harmonic comb at a quarter of the injected comb spacing. A fine-tuning of the detuning may allow the VCSEL to bifurcate to

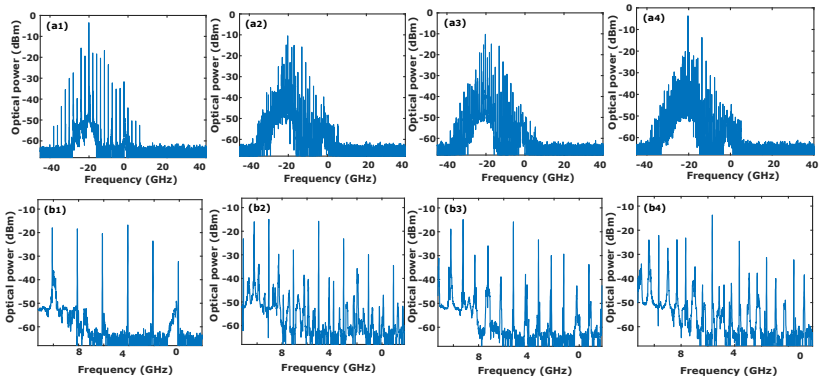

Fig. 6. Nonlinear dynamics when varying the detuning frequency for fixed comb spacing $\Omega = 2$ GHz and injected power $P_{inj} = 150$ µW. The VCSEL output shows: (a_1) new OFC at $\Delta\nu = -9.8$ GHz, (a_2) complex dynamics at $\Delta\nu = -10.8$ GHz,(a_3) harmonic comb at half of the injected comb spacing at $\Delta\nu = -11$ GHz, (a_4) harmonic comb at third of the injected comb spacing at $\Delta\nu = -11.4$ GHz. The optical spectra in (b_1), (b_2), (b_3), and (b_4) correspond to the zoom in of the spectra in (a_1), (a_2), (a_3), and (a_4), respectively.

a stable comb at a quarter of the injected comb spacing creating a new OFC with a comb spacing of 500 MHz instead of 2 GHz which is a useful tool for spectroscopy applications [30]. When we keep varying the detuning, a stable harmonics comb at half of the injected comb spacing takes place as shown in Fig. 6 (a_3). When further varying the detuning, the VCSEL output dynamics becomes complex. These complex dynamics lead to the appearance of new frequency lines at a specific position creating an optical spectrum regularly spaced corresponding to a new OFC with a comb spacing of 670 MHz as shown in Fig. 6 (a_4).

We now analyze the scenarios shown by the red arrow B in the mapping of Fig. 2 (b), for which the injected power required to switch on the normally depressed Y-PM is minimum, see Figure 7. These figures are obtained for a fixed comb spacing of $\Omega = 2$ GHz and detuning of $\Delta\nu = -17.7$ GHz. The frequency of the central line of the injected comb matches with the position of the Y-PM. When varying the injected power, the VCSEL output displays different dynamics. For lower injected power, the VCSEL shows an unlocked dynamics corresponding to Fig. 7 (a). The red arrow indicates the position of the central line of the injection comb. When the injected power is increased to $P_{inj} = 16$ µW, the polarization mode containing the maximum power switches from X-PM to the Y-PM. This switching is accompanied by the creation of new comb lines as shown in Fig. 7 (b). When we keep increasing the injected power, the VCSEL stabilizes on the new OFC dynamics while continuing to increase the number of output comb lines until reaching about 3 times the number of injected lines [Fig. 7 (c)]. From Fig. 7 (c) to Fig. 7 (d) the VCSEL bifurcates abruptly from a stable orthogonal comb dynamics to complex dynamics in which the two linear polarization modes are excited. Figure 7 (e) shows the case where an increase in injected power allows again a gradual elimination of the dominant mode of the VCSEL (X-PM) leading to a new dynamics corresponding to a harmonic comb. This harmonic comb is a new OFC with a repetition rate at half of the injected comb spacing, i.e., 1 GHz. From Fig. 7 (e), when we increase the injected power, the harmonic comb becomes more stable in the Y-PM mode with a decrease of the noise pedestal and the disappearance of the small quantity of power in X-PM. The harmonics frequency lines disappear with the injected power to give rise to a OFC with the same repetition rate as the injected comb as shown in Fig. 7 (f). The new comb shown in Fig. 7 (f) is more efficient in terms of the number of comb lines and flatness than the one

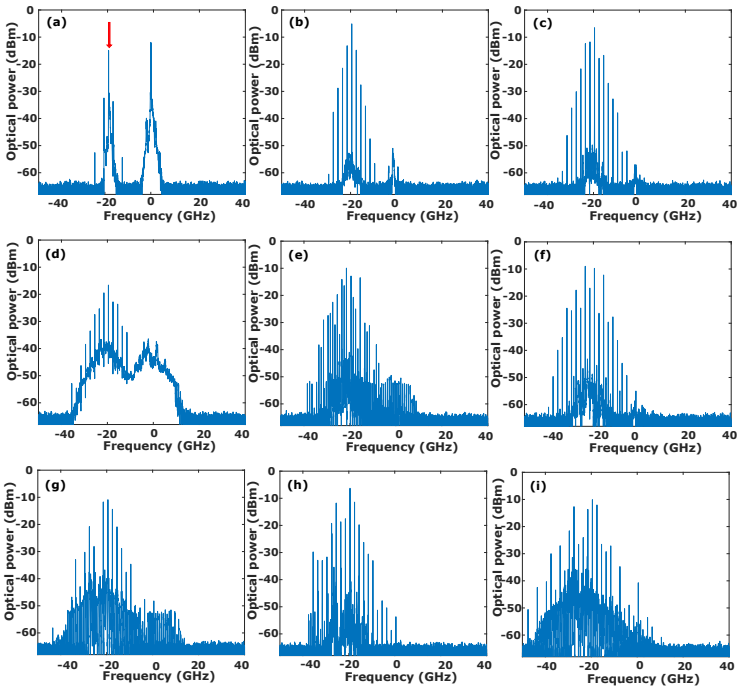

Fig. 7. Scenario B: Route to polarization switching with harmonics OFC generation for detuning close to the birefringence, i.e, frequency position of Y-PM, $\Delta\nu = -17.7$ GHz and for fixed $\Omega = 2$ GHz. When increasing the injected power, the VCSEL output shows the following dynamics: (a) Unlocked dynamics at $P_{inj} = 0.3$ µW, (b) and (c) PS with new frequency lines generations at $P_{inj} = 16$ µW and $P_{inj} = 32$ µW, respectively, (d) complex dynamics in both polarization modes at $P_{inj} = 40$ µW, (e) and (f) Unlocked time-periodic corresponding to a harmonics comb and comb at repetition of $\Omega = 2$ GHz in Y-PM at $P_{inj} = 56$ µW, and $P_{inj} = 64$ µW, respectively, (g) complex dynamics at $P_{inj} = 376$ µW, (h) OFC at $P_{inj} = 400$ µW, and (i) complex dynamics with comb lines at $P_{inj} = 696$ µW. The red arrow in optical spectrum of (a) indicates the position of the central injected comb line.

in Fig. 7 (c). Figure 7 (g) correspond to the complex dynamics, but with the presence of OFC lines. When further increasing the injected power, Fig. 7 (h) shows that the VCSEL output can be again a stable comb, much flatter, but with a simultaneous increase in the pedestal noise. In this region of comb dynamics, the noise pedestal decreases to achieve a minimum and then increase to destabilizes the comb with the injected power as shown in Fig. 7 (i). As demonstrated in [5] for the single-mode injection case in VCSEL, the comparison between Fig. 3 and Fig. 7 allows to conclude that the polarization switching depends on the injection parameters (injected power and detuning).

5. Two polarization frequency comb generation

The previous section has shown the possibility to tune the polarization of the VCSEL comb and to adjust the comb properties. Here we show how to optimize the extension of the OFC over the two polarization modes. Figure 8 shows the route to two polarization OFC generation. The injection parameters corresponding to this scenarios are indicated in red arrow C in the mapping of Fig. 2 (b). These optical spectra are obtained for fixed $\Delta\nu = -6.5$ GHz and $\Omega = 2$ GHz. When increasing the injected power [Fig. 8 (a), (b) and (c)], we observe an unlocked

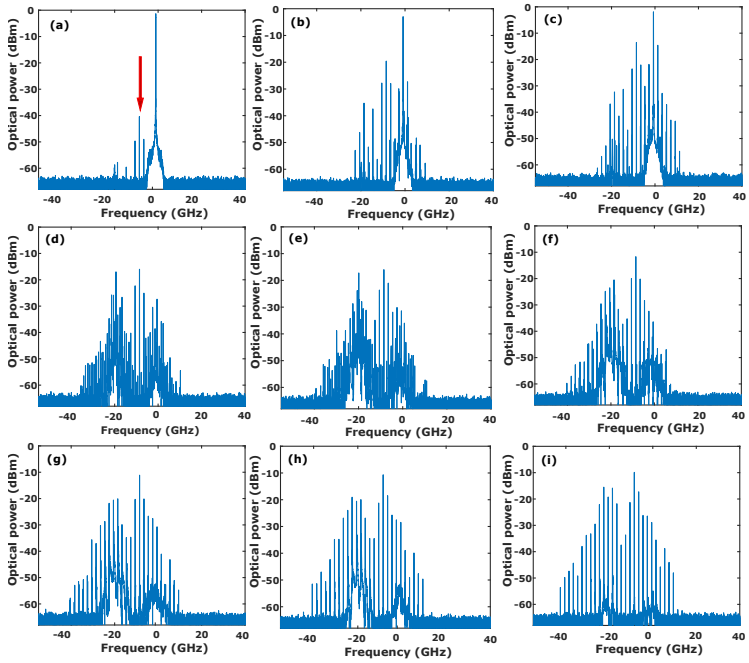

Fig. 8. Scenario C: Optical spectra of two polarization OFC dynamics for fixed comb spacing to $\Omega = 2$ GHz, and detuning $\Delta\nu = -6.5$ GHz. (a), (b) and (c), unlocked dynamics at $P_{inj} = 0.3$ µW, $P_{inj} = 80$ µW and $P_{inj} = 216$ µW, respectively, (d) incomplete PS at $P_{inj} = 224$ µW, (e) complex harmonic comb in both polarization modes at $P_{inj} = 408$ µW, (f) and (g) complex comb in both polarization modes at $P_{inj} = 520$ µW and $P_{inj} = 576$ µW, respectively, (h) and (i) comb in both polarization modes $P_{inj} = 600$ µW and $P_{inj} = 640$ µW, respectively. The red arrow in optical spectrum of (a) indicates the position of the central injected comb line.

dynamics with excitation of both polarization modes. Some comb lines start to appear around the Y-PM polarization mode. The nonlinear dynamics generated in the X-PM is strong enough to excite the Y-PM in Fig. 8 (d). Within the range of injected power leading to excitation of the two polarization modes, harmonic OFC in both polarization modes is observed. Once the two polarization modes are excited, the VCSEL output is a succession of complex dynamics and harmonic OFC in both polarization modes when increasing the injected power as shown in Fig. 8 (d) and (e). When we keep increasing the injected power, new frequency lines start to appear in both polarization modes making the VCSEL output a noisy OFC [Fig. 8 (f)]. The unstable comb dynamics disappears as we increase the injected power giving rise to an OFC with a strong noise pedestal. Figure 8 (h) and (i) show the situation in which an increase in the power leads to the suppression of noise pedestal and a significant increase in the number of the output comb lines.

Figure 9 shows the polarization-resolved optical spectrum corresponding to Fig. 8 (i). Figure 9 (a), (b), and (c) present the optical spectra corresponding to X-PM, Y-PM, and the total output power. We observe the comb dynamics in the optical spectra of both polarization. The CNR of the X-PM is around 40 dB which is close to the maximum found in the gain switching VCSEL-based OFC [44]. Each of these polarization comb has the necessary performance to be used distinctly as a multiple channels light source.

Figure 10 (a) analyzes the power spectra of Fig. 4 (e). We examine the power spectrum on an electrical spectrum analyser (ESA). A high speed photodiode is placed at the input of the (ESA). We observe that the frequency lines are regularly separated by 2 GHz corresponding to the comb

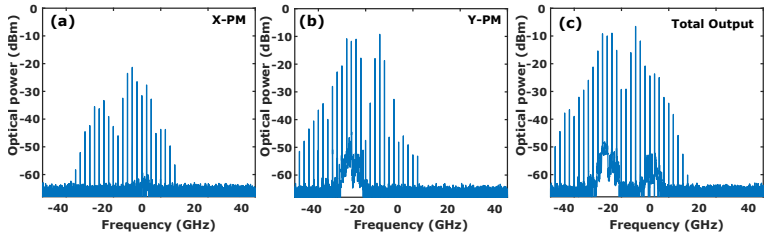

Fig. 9. Polarization resolved spectra corresponding to the comb evolution in scenarios C. (a), (b), (c), optical spectra of X-PM, Y-PM and total output power, respectively for fixed P_{inj} = 552.8 μW and $\Delta\nu = -6.8$ GHz.

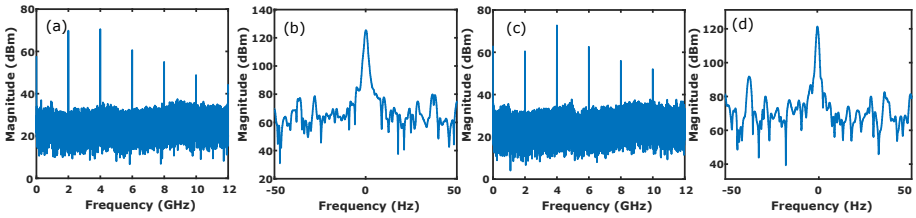

Fig. 10. (a) the power spectrum of the comb shown in Fig. 4 (e) and the corresponding zoom in (b). (c) the power spectrum of the comb in Fig. 9 (c) and the corresponding zoom in (d).

spacing. We then computed the linewidth as in [45,46]. We tuned the ESA to select the frequency line at 2 GHz as shown in Figure 10 (b). The -3 dB width is found to be approximatively 1.1 Hz (3.4 Hz at -20 dB), which is much narrower than the one of the injected comb (1.2 Hz), suggesting that the comb lines are coherent. Figure 10 (c) corresponds to the power spectrum of the two-polarization comb of Fig. 9 (c). To address the coherence between X-PM and Y-PM comb lines, a P.C at 45° between X-PM and Y-PM was placed at the input of the photodiode. The lines in the power spectrum are separated by 2 GHz. We did not observe any additional beat note, which confirms that the comb lines in X-PM are locked to the ones in Y-PM, i.e., there is no frequency shift between the comb lines in X-PM and Y-PM. By varying the detuning we can tune the frequency shift between X-PM and Y-PM combs, therefore unlocking the two-polarization combs leading to the appearance of a beat note at the frequency shift between the X-PM and Y-PM comb. There is approximately 1 GHz of area of detuning frequency, where the locking between the orthogonal comb is observed. The linewidth computed from Fig. 10 (d) at -3 dB is found to be approximately 1 Hz (2.4 Hz at -20dB) which indicates the coherence between the two polarization comb lines. The linewidth found is of the same order of magnitude as the one of the dual-polarization comb obtained recently with a more sophisticated scheme using two separate electro-optical modulators [47].

As we have seen in the previous cases, a careful tuning of the injection parameters such that the VCSEL gets close or not to the PS point is used to enable either a single polarization comb (Fig. 4 (e)) or a two polarization comb (Fig. 4 (h) and Fig. 8 (i)). Both the nonlinear dynamics induced extension of the number of the comb lines, and the polarization competition induced by the orthogonal optical injection, play a role in equilibrating or not the power in the X-PM and Y-PM combs. Figure 11 highlights that the onset of such a broadband two polarization comb is possible independently of the comb spacing relative to the X-Y birefringence induced frequency splitting. Figures 11 (a), (b), and (c) correspond to Ω = 500 MHz, Ω = 2 GHz, and Ω = 4 GHz, respectively.

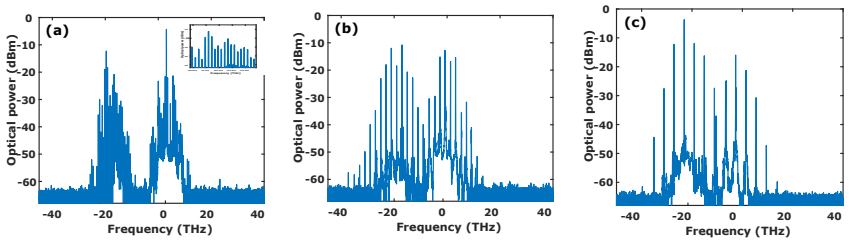

Fig. 11. Optical spectra revealing the nonlinear dynamics of two polarization OFC when varying both the comb properties and the injection parameters. (a), (b), ad (c) are obtained for $\Omega = 500$ MHz, $\Omega = 2$ GHz, and $\Omega = 4$ GHz. The injected light parameters are (a) $\Delta\nu = -23.2$ GHz and $P_{inj} = 54$ µW, (b) $\Delta\nu = -15.7$ GHz and $P_{inj} = 72$ µW, and (c) $\Delta\nu = -16.9$ GHz and $P_{inj} = 96$ µW.

6. Tailoring the comb properties

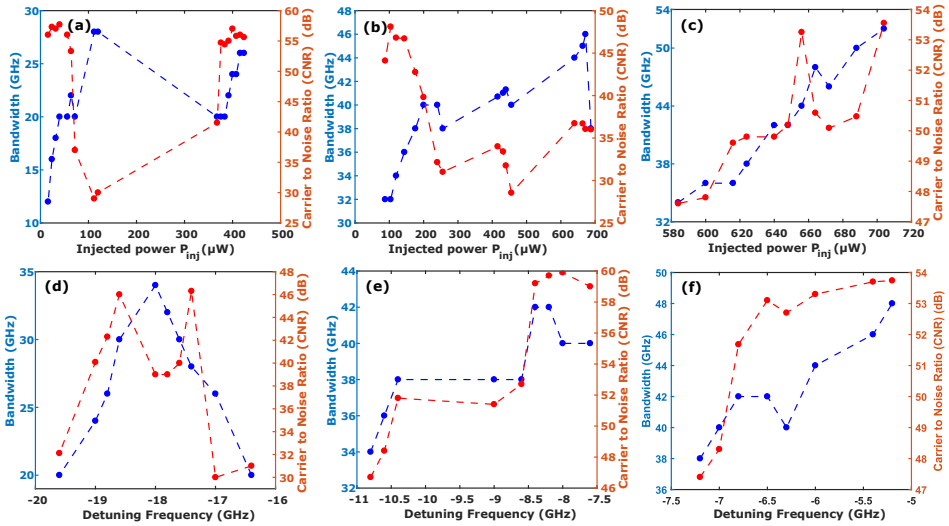

Fig. 12. Control of OFC properties with the injection parameters for a fixed comb spacing of $\Omega = 2$ GHz . The curves in blue and red in each map correspond to the bandwidth on the left vertical axis and the CNR on the right vertical axis, respectively. (a), (b) and (c) are obtained for fixed detuning $\Delta\nu = -18.8$ GHz, $\Delta\nu = -11.2$ GHz, and $\Delta\nu = -6.5$ GHz, respectively when varying the injected power. (d), (e) and (f) are obtained for fixed injected power $P_{inj} = 120$ µW, $P_{inj} = 608$ µW, and $P_{inj} = 640$ µW, respectively.

We qualify the generated comb quality by the bandwidth (number of lines) and Carrier to Noise Ratio (CNR). The CNR is the difference, in dB, between the maximum amplitude in the optical spectrum and the noise level as shown in Fig. 3 (c). Figure 12 analyzes the performance of the combs corresponding to an example of the bifurcation scenario A, B and C (in Figure 2). The curves in blue and red in each map correspond to the bandwidth on the left vertical axis and the CNR on the right vertical axis, respectively. Figures 12 (a), (b) and (c) correspond to comb properties of an example of the bifurcations scenario B, A, and C, respectively, for fixed detuning $\Delta\nu = -18.8$ GHz, $\Delta\nu = -11.2$ GHz, and $\Delta\nu = -6.5$ GHz. For the computation of

comb bandwidth, we consider an output line when its amplitude lies above -30 dB from the maximum amplitude. When the total intensity spectrum shows a dip, the bandwidth is estimated from the separate bandwidth of X-PM and Y-PM spectra. As we learned from our previous work [28, 29], when increasing the injected power, the comb bandwidth increases as shown in Fig. 12 (a) and (b). When varying the injected power for fixed detuning, several distinct comb regions can be observed as shown in Fig. 4 and Fig. 7. The discontinuities in the evolution of the bandwidth are due to the transition between these comb regions. At the boundaries of each comb region, the bandwidth and the CNR decrease and then increase again with the injected power. Interestingly, Fig. 12 (a) and (b) show that the best value of CNR is found close to the PS point. As we can see in the Fig. 7 (b), (c) and (f), where the CNR is 54.48 dB, 53.36 dB and 49.26 dB, respectively, the decrease of the CNR is explained by the increase of the comb pedestal due to comb dynamical instabilities. Figure 12 (c) shows an increase of both the comb bandwidth and the CNR. As we can see in Fig. 8 (g), (h) and (i), when we are inside the comb region, the comb pedestal decreases with the injected power until almost disappearing accompanied by the increase of the bandwidth through the increase of the number of total output lines.

Figure 12 (d), (e), and (f) analyze the comb bandwidth on the left vertical axis and the CNR on the right vertical axis for P_{inj} = 108 μW, P_{inj} = 608 μW, and P_{inj} = 640 μW, respectively, when varying the detuning frequency. Figure 12 (d) shows that the CNR and the comb bandwidth start to get maximums as the detuning approaches a specific value $\Delta\nu = -17.7$ GHz,i.e., when the central injected comb line is close to the frequency position of the normally depressed polarization mode Y-PM. This is true whatever is the injected power. In Fig. 12 (d) we observe a discontinue increasing of both the comb bandwidth and the CNR when varying the detuning. As shown in Fig. 12 (a) and (b), the CNR is best close to the PS point. When varying the detuning to be close to 0, the noise pedestal decreases accompanied by an increase of the bandwidth through the increase of the amplitude of the comb lines. When the detuning is close to a switching point, the CNR gets its best value, which is in agreement with Fig. 12 (a) and (b). Figure 12 (f) plots the comb performance for the bifurcation scenario C (See Fig. 2 (b)). The comb bandwidth and the CNR both increase with the detuning. We checked that when the detuning is being close to 0, the contribution of X-PM in the total output increases due to the fact that the two polarization modes are excited with comparable power. It has been demonstrated very recently that the CNR and the bandwidth of the OFC based on gain switching laser do not increase together with the injected power [31]. Figure 12 (c) and (f) show the possibility to increase together, the comb bandwidth and the CNR when varying both the detuning frequency and the injected power. It is also worth emphasizing that the CNRs obtained here are 3 times higher than the one typically required for spectroscopy measurement which is around 20 dB [30, 43].

7. Conclusion

In conclusion, we have experimentally analyzed the nonlinear polarization dynamics of VCSEL subject to optical frequency comb injection. By tuning both the polarization and the injection parameters, we have enabled an optical control of the comb spacing, the Carrier to Noise Ratio (CNR), and the polarization of the optical frequency comb of the VCSEL output light. Similar to optical injection of a fixed frequency light, we observe that polarization switching (PS) plays a crucial role in the dynamics. The best value of the CNR is found to be close to the PS point. A sweep of the detuning of the injected light shows a significant increase of both the CNR and the comb bandwidth for a detuning of $\Delta\nu = -17.7$ GHz, i.e., when the injection central comb line has a frequency close to that of the normally depressed VCSEL polarization mode. The best comb performance is observed when the nonlinear dynamics induced comb extension combines with the excitation of the two polarization modes in the VCSEL since it is a way to further improve the comb bandwidth. Our results show the possibility of controlling the comb properties to adapt it to several applications. The generation of the two polarization comb and the tailoring

of the comb properties are the first steps towards dual-polarization comb generation and related application in dual comb spectroscopy.

Funding

The presented study is funded by the Chaire Photonique: Ministère de l'Enseignement Supérieur, de la Recherche et de l'Innovation; Région Grand-Est; Département Moselle; European Regional Development Fund (ERDF); GDI Simulation; CentraleSupélec; Fondation CentraleSupélec. Fondation Supélec and Metz Metropole. Fonds Wetenschappelijk Onderzoek (FWO) Vlaanderen Project No.G0E5819N.

Data availability: Data underlying the results presented in this paper are not publicly available at this time but may be obtained from the authors upon reasonable request.

Disclosures. The authors declare no conflicts of interest.

References

1. A. Hugi, G. Villares, S. Blaser, H. Liu, and J. Faist, "Mid-infrared frequency comb based on a quantum cascade laser," Nature **492**, 229–233 (2012).
2. J. Davila-Rodriguez, K. Bagnell, and P. J. Delfyett, "Frequency stability of a 10 ghz optical frequency comb from a semiconductor-based mode-locked laser with an intracavity 10,000 finesse etalon," Opt. letters **38**, 3665–3668 (2013).
3. T. J. Kippenberg, R. Holzwarth, and S. A. Diddams, "Microresonator-based optical frequency combs," science **332**, 555–559 (2011).
4. C. He, S. Pan, R. Guo, Y. Zhao, and M. Pan, "Ultraflat optical frequency comb generated based on cascaded polarization modulators," Opt. letters **37**, 3834–3836 (2012).
5. M. Sciamanna and K. Panajotov, "Route to polarization switching induced by optical injection in vertical-cavity surface-emitting lasers," Phys. Rev. A **73**, 023811 (2006).
6. J. B. Altés, I. Gatare, K. Panajotov, H. Thienpont, and M. Sciamanna, "Mapping of the dynamics induced by orthogonal optical injection in vertical-cavity surface-emitting lasers," IEEE journal quantum electronics **42**, 198–207 (2006).
7. K. Panajotov, M. Sciamanna, M. A. Arteaga, and H. Thienpont, "Optical feedback in vertical-cavity surface-emitting lasers," IEEE J. Sel. Top. Quantum Electron. **19**, 1700312–1700312 (2012).
8. M. Ozaki, H. Someya, T. Mihara, A. Uchida, S. Yoshimori, K. Panajotov, and M. Sciamanna, "Leader-laggard relationship of chaos synchronization in mutually coupled vertical-cavity surface-emitting lasers with time delay," Phys. Rev. E **79**, 026210 (2009).
9. M. Sciamanna, K. Panajotov, H. Thienpont, I. Veretennicoff, P. Mégret, and M. Blondel, "Optical feedback induces polarization mode hopping in vertical-cavity surface-emitting lasers," Opt. letters **28**, 1543–1545 (2003).
10. A. Hurtado, A. Quirce, A. Valle, L. Pesquera, and M. J. Adams, "Nonlinear dynamics induced by parallel and orthogonal optical injection in 1550 nm vertical-cavity surface-emitting lasers (vcsels)," Opt. express **18**, 9423–9428 (2010).
11. R. Al-Seyab, K. Schires, N. A. Khan, A. Hurtado, I. D. Henning, and M. J. Adams, "Dynamics of polarized optical injection in 1550-nm vcsels: theory and experiments," IEEE J. Sel. Top. Quantum Electron. **17**, 1242–1249 (2011).
12. L. Olejniczak, K. Panajotov, H. Thienpont, M. Sciamanna, A. Mutig, F. Hopfer, and D. Bimberg, "Polarization switching and polarization mode hopping in quantum dot vertical-cavity surface-emitting lasers," Opt. express **19**, 2476–2484 (2011).
13. A. Valle, M. Sciamanna, and K. Panajotov, "Irregular pulsating polarization dynamics in gain-switched vertical-cavity surface-emitting lasers," IEEE J. Quantum Electron. **44**, 136–143 (2008).
14. A. Valle, M. Sciamanna, and K. Panajotov, "Nonlinear dynamics of the polarization of multitransverse mode vertical-cavity surface-emitting lasers under current modulation," Phys. Rev. E **76**, 046206 (2007).
15. M. Virte, K. Panajotov, H. Thienpont, and M. Sciamanna, "Deterministic polarization chaos from a laser diode," Nat. Photonics **7**, 60 (2013).
16. I. Gatare, J. Buesa, H. Thienpont, K. Panajotov, and M. Sciamanna, "Polarization switching bistability and dynamics in vertical-cavity surface-emitting laser under orthogonal optical injection," Opt. quantum electronics **38**, 429–443 (2006).
17. A. Quirce, A. Popp, F. Denis-le Coarer, P. Pérez, Á. Valle, L. Pesquera, Y. Hong, H. Thienpont, K. Panajotov, and M. Sciamanna, "Analysis of the polarization of single-mode vertical-cavity surface-emitting lasers subject to parallel optical injection," JOSA B **34**, 447–455 (2017).
18. F. Denis-le Coarer, A. Quirce, P. Pérez, A. Valle, L. Pesquera, M. Sciamanna, H. Thienpont, and K. Panajotov, "Injection locking and polarization switching bistability in a 1550 nm vcsel subject to parallel optical injection," IEEE J. Sel. Top. Quantum Electron. **23**, 1–10 (2017).

19. A. Quirce, P. Pérez, A. Popp, Á. Valle, L. Pesquera, Y. Hong, H. Thienpont, and K. Panajotov, "Polarization switching and injection locking in vertical-cavity surface-emitting lasers subject to parallel optical injection," Opt. letters **41**, 2664–2667 (2016).
20. A. D. Ellis and F. G. Gunning, "Spectral density enhancement using coherent wdm," IEEE Photonics Technol. Lett. **17**, 504–506 (2005).
21. F. Peters and A. Ellis, "Integrated optical comb source system and method," (2013). US Patent 8,488,640.
22. B. Lingnau, K. Shortiss, F. Dubois, F. H. Peters, and B. Kelleher, "Universal generation of devil's staircases near hopf bifurcations via modulated forcing of nonlinear systems," Phys. Rev. E **102**, 030201 (2020).
23. R. Desmet and M. Virte, "Laser diodes with modulated optical injection: towards a simple signal processing unit?" J. Physics: Photonics **2**, 025002 (2020).
24. Y. Lu, W. Zhang, B. Xu, X. Fan, Y. Sun, and Z. He, "Directly modulated vcsels with frequency comb injection for parallel communications," J. Light. Technol. (2020).
25. M. AlMulla, "Microwave frequency comb generation through optical double-locked semiconductor lasers," Optik **223**, 165506 (2020).
26. K. Shortiss, B. Lingnau, F. Dubois, B. Kelleher, and F. H. Peters, "Harmonic frequency locking and tuning of comb frequency spacing through optical injection," Opt. Express **27**, 36976–36989 (2019).
27. Y. Doumbia, T. Malica, D. Wolfersberger, K. Panajotov, and M. Sciamanna, "Frequency comb customization by controlling the optical injection dynamics," in *Semiconductor Lasers and Laser Dynamics IX,* vol. 11356 (International Society for Optics and Photonics, 2020), p. 113560G.
28. Y. Doumbia, T. Malica, D. Wolfersberger, K. Panajotov, and M. Sciamanna, "Nonlinear dynamics of a laser diode with an injection of an optical frequency comb," Opt. Express **28**, 30379–30390 (2020).
29. Y. Doumbia, T. Malica, D. Wolfersberger, K. Panajotov, and M. Sciamanna, "Optical injection dynamics of frequency combs," Opt. Lett. **45**, 435–438 (2020).
30. B. Jerez, P. Martín-Mateos, E. Prior, C. de Dios, and P. Acedo, "Gain-switching injection-locked dual optical frequency combs: characterization and optimization," Opt. letters **41**, 4293–4296 (2016).
31. A. Quirce, A. Rosado, J. Díez, A. Valle, A. Pérez-Serrano, J.-M. G. Tijero, L. Pesquera, and I. Esquivias, "Nonlinear dynamics induced by optical injection in optical frequency combs generated by gain-switching of laser diodes," IEEE Photonics J. **12**, 1–14 (2020).
32. E. Prior, C. De Dios, R. Criado, M. Ortsiefer, P. Meissner, and P. Acedo, "Dynamics of dual-polarization vcsel-based optical frequency combs under optical injection locking," Opt. letters **41**, 4083–4086 (2016).
33. A. Quirce, C. De Dios, A. Valle, and P. Acedo, "Vcsel-based optical frequency combs expansion induced by polarized optical injection," IEEE J. Sel. Top. Quantum Electron. **25**, 1–9 (2018).
34. A. Quirce, C. de Dios, A. Valle, E. Prior, L. Pesquera, K. Panajotov, J. Palací, P. Meissner, and P. Acedo, "Vcsel-based optical frequency combs: Study of its polarization dynamics under gain switching and polarization selective optical injection locking," in *2018 20th International Conference on Transparent Optical Networks (ICTON),* (IEEE, 2018), pp. 1–4.
35. H. Moon, E. Kim, S. Park, and C. Park, "Selection and amplification of modes of an optical frequency comb using a femtosecond laser injection-locking technique," Appl. physics letters **89**, 181110 (2006).
36. A. Gavrielides, "Comb injection and sidebands suppression," IEEE J. Quantum Electron. **50**, 364–371 (2014).
37. H. Y. Ryu, S. H. Lee, E. B. Kim, H. S. Suh, and H. S. Moon, "A discretely tunable multifrequency source injection locked to a spectral-mode-filtered fiber laser comb," Appl. Phys. Lett. **97**, 141107 (2010).
38. A. S. Tistomo and S. Gee, "Laser frequency fixation by multimode optical injection locking," Opt. express **19**, 1081–1090 (2011).
39. Z. Liu and R. Slavík, "Optical injection locking: From principle to applications," J. Light. Technol. **38**, 43–59 (2019).
40. Y. Xu, Y. Lin, A. Nielsen, I. Hendry, S. Coen, M. Erkintalo, H. Ma, and S. G. Murdoch, "Harmonic and rational harmonic driving of microresonator soliton frequency combs," Optica **7**, 940–946 (2020).
41. Y. Huang, Q. Li, J. Han, Z. Jia, Y. Yu, Y. Yang, J. Xiao, J. Wu, D. Zhang, Y. Huang, Q. Weiping, and Q. Guanshi, "Temporal soliton and optical frequency comb generation in a brillouin laser cavity," Optica **6**, 1491–1497 (2019).
42. M. W. Day, M. Dong, B. C. Smith, R. C. Owen, G. C. Kerber, T. Ma, H. G. Winful, and S. T. Cundiff, "Simple single-section diode frequency combs," APL Photonics **5**, 121303 (2020).
43. C. Quevedo-Galán, V. Durán, A. Rosado, A. Pérez-Serrano, J. Tijero, and I. Esquivias, "Gain-switched semiconductor lasers with pulsed excitation and optical injection for dual-comb spectroscopy," Opt. Express **28**, 33307–33317 (2020).
44. A. Quirce, C. de Dios, A. Valle, and P. Acedo, "Vcsel-based optical frequency combs: Expansion of the optical span under arbitrary polarized optical injection," in *2019 21st International Conference on Transparent Optical Networks (ICTON),* (IEEE, 2019), pp. 1–4.
45. J. Hillbrand, D. Auth, M. Piccardo, N. Opačak, E. Gornik, G. Strasser, F. Capasso, S. Breuer, and B. Schwarz, "In-phase and anti-phase synchronization in a laser frequency comb," Phys. review letters **124**, 023901 (2020).
46. V. Moskalenko, J. Koelemeij, K. Williams, and E. Bente, "Study of extra wide coherent optical combs generated by a qw-based integrated passively mode-locked ring laser," Opt. letters **42**, 1428–1431 (2017).
47. G. Millot, S. Pitois, M. Yan, T. Hovhannisyan, A. Bendahmane, T. W. Hänsch, and N. Picqué, "Frequency-agile dual-comb spectroscopy," Nat. Photonics **10**, 27–30 (2016).